Pathways for wintertime deposition of anthropogenic light-absorbing particles on the Central Andes cryosphere

Rémy Lapere, Sylvain Mailler, Laurent Menut, Nicolás Huneeus

Pathways for wintertime deposition of anthropogenic light-absorbing particles on the Central Andes cryosphere

Rémy Lapere[a,*], Sylvain Mailler[a,b], Laurent Menut[a], Nicolás Huneeus[c]

[a] *Laboratoire de Météorologie Dynamique, IPSL, École Polytechnique, Institut Polytechnique de Paris, ENS, Université PSL, Sorbonne Université, CNRS, Palaiseau, France*
[b] *École des Ponts, Université Paris-Est, 77455 Champs-sur-Marne, France*
[c] *Department of Geophysics, Universidad de Chile, Santiago, Chile*

Abstract

Ice and snow in the Central Andes contain significant amounts of light-absorbing particles such as black carbon. The consequent accelerated melting of the cryosphere is not only a threat from a climate perspective but also for water resources and snow-dependent species and activities, worsened by the mega-drought affecting the region since the last decade. Given its proximity to the Andes, emissions from the Metropolitan Area of Santiago, Chile, are believed to be among the main contributors to deposition on glaciers. However, no evidence backs such an assertion, especially given the usually subsident and stable conditions in wintertime, when the snowpack is at its maximum extent. Based on high-resolution chemistry-transport modeling with WRF-CHIMERE, the present work shows that, for the month of June 2015, up to 40% of black carbon dry deposition on snow or ice covered areas in the Central Andes downwind from the Metropolitan area can be attributed to emissions from Santiago. Through the analysis of aerosol tracers we determine (i) that the areas of the Metropolitan Area where emissions matter most when it comes to export towards glaciers are located in Eastern Santiago near the foothills of the Andes, (ii) the crucial role of the network of Andean valleys that channels pollutants up to remote locations near glaciers, following gentle slopes. A direct corollary is that severe urban pollution, and deposition of impurities on the Andes, are anti-correlated phenomena. Finally, a two-variable meteorological index is developed that accounts for the dynamics of aerosol export towards the Andes, based on the zonal wind speed over the urban area, and the vertical diffusion coefficient in the valleys close to ice and snow covered terrain. Numerous large urban areas are found along the Andes so that the processes studied here can shed light on similar investigations for other glaciers-dependent Andean regions.

Keywords: Black Carbon, Chemistry-transport, Urban pollution, Cryosphere

1. Introduction

The chapter on High Mountain Areas, from the IPCC's Special Report on the Ocean and Cryosphere in a Changing Climate (SROCC) (Hock et al., 2019) highlights the threats posed by the feedback associated with deposition of light absorbing particles on snow and glaciers, that induce surface air warming along with accelerated snow cover reduction. Recent studies over the Tibetan Plateau show that light-absorbing particles are responsible for about 20% of the albedo reduction of glaciers at the end of winter, corresponding to a radiative forcing of up to hundreds of W m^{-2}, hence accelerating their melting during the warmer season (Zhang et al., 2017; Kang et al., 2020). In addition to a positive radiative feedback on climate, local impacts on water resources, population security, ecosystems, infrastructure and tourism are also at stake.

Glaciers in Chile have been shrinking over the recent decades, in particular in the Central Chilean Andes (32°S to 36°S) where large glaciers feed valleys rich in agriculture and large populated centers such as Santiago, Chile's capital (Pellicciotti et al., 2013). Although the role of anthropogenic black carbon (BC) on the retreat of glaciers has not been established for South American glaciers, previous studies suggest that deposition of BC on snow can affect the length of the snow cover season in the Northern hemisphere reducing its duration by up to 10 days in boreal and temperate regions (Ménégoz et al., 2013) and up to 8 days in the Himalayas (Ménégoz et al., 2014). The current mega-drought in Central Chile exacerbates the retreat of the Central Andean glaciers and threatens the sustainability of water resources in the region (Garreaud et al., 2017, 2019). The stakes are thus high for urban areas neighboring the Andes cordillera. In this context, BC deposition on the Central Andes glaciers represents an additional burden, and as the management of water resources becomes paramount in the region for the coming years, a detailed knowledge of the processes and sources leading to the presence of BC in glaciers is essential.

A likely contribution of anthropogenic pollution to the observed retreat of glaciers in the Central Andes was found (Molina et al., 2015; Rowe et al., 2019). In particular, the significant amount of atmospheric pollutants emitted in Santiago, Chile is hypothesized to influence ice composition in nearby glaciers (Cereceda-Balic et al., 2011; Rowe et al., 2019). Indeed, the city regularly faces high levels of fine particulate matter pollution, of which BC, in wintertime, mainly due to mas-

*remy.lapere@lmd.polytechnique.fr

sive emissions from wood burning for residential heating and diesel-fueled vehicles (Barraza et al., 2017), but also to episodic strong emissions from barbecue cooking (Lapere et al., 2020). Nevertheless, no evidence was found so far to confirm that BC emissions from Santiago are able to deposit on the Central Andes glaciers, particularly given the subsident conditions associated with a shallow stable boundary layer and a persistent inversion over the city observed during winter months (Garreaud, 2009), when most residential wood burning emissions occur and snow extent is at its maximum. Furthermore, Santiago is only 500 m above sea level, while nearby Andean mountains reach altitudes as high as 5800 m, which represents a huge obstacle to go over for these stable, non-convective air masses. In particular, Cordova et al. (2015) found that at the beginning of spring 2014, air masses reaching an Andean valley southeast of Santiago barely interacted with urban air from the city. On the other hand, Gramsch et al. (2020) has shown recently that for the northern part of Santiago, emissions from the urban area can contribute significantly to atmospheric concentrations observed higher up in the cordillera, with limited export in wintertime compared to summertime.

Studies over the Himalayas and the Alps show that an effective pathway for deposition of anthropogenic particles on glaciers is channeling through valleys (Ming et al., 2012; Diémoz et al., 2019a). However, wintertime conditions lead to a minimum intensity of this phenomenon (Diémoz et al., 2019b). Also, during fair weather convective days, vertical export of air masses from the boundary layer into the free troposphere can occur through topographic venting (Henne et al., 2004). Again, this mechanism is less active under stable cold conditions. Holmes et al. (2015) suggest enhanced vertical mixing over complex terrain in wintertime under cloudy conditions, in the western United States. Nonetheless, given the quite unique configuration of the Andes cordillera, the processes at play for a potential wintertime export of pollutants from Santiago basin up to the Andean glaciers are not well known, and are investigated in this study.

The objective of this work is to provide a first assessment of the burden of Santiago's emissions on BC deposition over the Central Andean snowpack, and to understand why this contribution can be significant while the mainly stable meteorological conditions observed in wintertime would lead to think that the export of pollutants is prevented. To do so, a combination of observations and chemistry-transport modeling with WRF-CHIMERE is used to determine the amount of BC deposition on glaciers attributable to emissions from Santiago and the associated pathways.

2. Data and methods

The present work relies for a large part on chemistry-transport modeling with WRF-CHIMERE. Atmospheric composition and meteorological measurements are also used, for analysis purposes as well as for assessing the quality of the simulations. These two components are described hereafter.

2.1. Observational data

Time series of hourly surface measurements of meteorology and air quality are extracted from the automated air quality monitoring network of Santiago (SINCA - `https://sinca.mma.gob.cl/index.php/region/index/id/M`, last access 28 April 2020). Climatological daily rainfall and temperature data at DMC is issued from the Chilean Weather Service (DMC, from Spanish *Direccion Meteorológica de Chile*) and accessible from the Chilean Center for Climate Science and Resilience through their online database *Explorador Climático* (CR2 - `http://explorador.cr2.cl/`, last access 28 April 2020). For the analysis of the model's ability to reproduce a specific transport event with complex topography, additional data from a dedicated one-week campaign carried out in Santiago and the adjacent Maipo canyon, including vertical profiles of BC, have been used. This campaign was conducted from Monday 20 until Sunday 26 July 2015. In each one of the three sites defined during the campaign (locations DMC downtown Santiago, VZC at the entrance of the Maipo canyon, and GYC inside the meridional branch of the canyon - a map is provided later on), hourly surface measurements of standard meteorological parameters and PM_{10} concentration were conducted. In addition, vertical profile measurements of BC (via a mini-aethalometer) and standard meteorological parameters are available up to 1 km above ground, from tethered balloon, every 3 hours.

2.2. Modeling setup

The chemistry-transport simulations use the Weather Research and Forecasting (WRF) mesoscale numerical weather model (Skamarock et al., 2008) to simulate the meteorological fields, and CHIMERE to compute chemistry and transport. Anthropogenic emissions are taken from the EDGAR-HTAP inventory. Two simulation domains are considered and described in Figure 1 and Table 1, with a coarse domain at a 5 km spatial resolution including Central Chile (referred to as CC5 hereafter), and a nested domain focusing on Santiago area at a 1 km resolution (referred to as STG1 hereafter). The model configuration used in this study is presented in Table A.1. WRF is applied to 46 vertical levels up to 50 hPa, in a two-way nested fashion. Initial and boundary conditions used are from the NCEP FNL analysis, with a 1° by 1° spatial resolution and 6-hour temporal resolution, from the Global Forecast System (NCEP, 2000). Land-use and orography are based on the modified IGBP MODIS 20-category database with 30 sec resolution (Friedl et al., 2010). CHIMERE is a Eulerian 3-dimensional regional Chemistry-Transport Model, able to reproduce gas-phase chemistry, aerosols formation, transport and deposition. In this study the 2017 version of CHIMERE is used (Mailler et al., 2017). The configuration is described in Table A.1. The EDGAR HTAP V2 dataset provides the anthropogenic emissions inventory, which consists of 0.1° gridded maps of air pollutant emissions for the year 2010 (Janssens-Maenhout et al., 2015). A downscaling is applied to this inventory based on land-use characteristics, and monthly emissions are split in time down to daily/hourly rates following the methodology of Menut et al. (2013).

Domain	Horizontal resolution	Purpose	Key output
CC5	5km (100x200 grid points)	Scenario on BC urban emissions	Contribution of BC from Santiago to deposition on glaciers
STG1	1km (100x100 grid points)	High resolution transport of tracers without chemistry	Pathways of aerosols from Santiago to the glaciers

Table 1: Description of CC5 and STG1 domains and their purposes. Both are centered on Santiago.

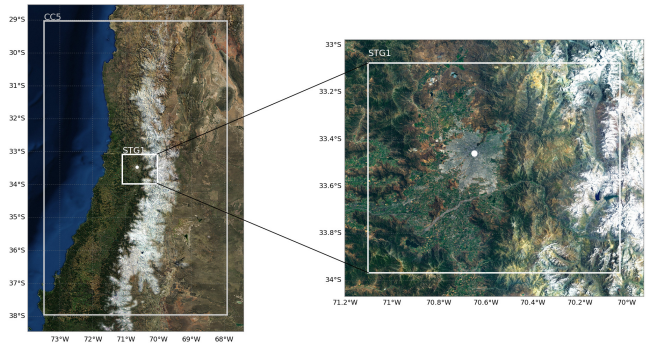

Figure 1: Left: coarse simulation domain at 5 km resolution - CC5. Right: nested domain at 1 km resolution - STG1. In both maps the white dot shows the location of downtown Santiago. Map background layer: Imagery World 2D, ©2009 ESRI.

The simulated period is 16 June to 31 July 2015. The period from 16 June to 30 June is used for spin-up and thus not analyzed. The choice to simulate the month of July 2015 is justified by the availability of dedicated measurements evidencing some of the processes studied here on the one hand, and on the other hand this month of the year is interesting for its combination of a large snow cover and high pollutants emissions at the same time. In June, pollution levels are similar but the extent of the snow cover is lesser, while August shows a more developed snowpack but less pollution in the city. In addition, meteorological conditions for July 2015 are climatologically typical of July, with daily mean, maximum and minimum temperatures in downtown Santiago of 9 °C, 12.6 °C and 5.5 °C, respectively, to be compared with the 2000-2019 median values of 8.4 °C, 12.1 °C and 4.3 °C respectively (Fig. A.1a). Precipitation in Santiago is also well in the range of the 21st century values with a daily mean at 1.2 mm close to the recorded 1.1 mm median over the last 20 years (Fig. A.1a). As for the wind regime, the mountain-valley circulation induced dipole of south-westerlies and easterlies in Santiago is consistent, with similar average wind speeds along these two main directions for the climatology and July 2015 (Fig. A.1b and A.1c, respectively). Simulation scores for meteorology and atmospheric composition, against observations at stations of the urban area, can be found in Tables A.2, A.3 and A.4. Surface wind and temperature, as well as vertical profiles for these two variables decently reproduce observations for several locations in Santiago. Thermal inversions are also successfully captured. Concentrations of $PM_{2.5}$ simulated in the CC5 case are in reasonable agreement with surface observations in the Metropolitan Area of Santiago.

For the CC5 domain, two simulations are performed. One with a full emissions inventory - referred to as baseline case or BS in the continuation - and one with an inventory setting emissions from Santiago area to zero - contribution case or CS. The comparison of these two simulations yields the share of emissions from Santiago in the atmospheric composition and deposition of pollutants in the region. As an example, the emission inventory extracted from EDGAR HTAP used for BC is provided in Figure 2a. The black rectangle on the inventory map defines the limit of the grid points belonging to the Metropolitan area of Santiago. The model points inside this zone see their emission rates of BC set to zero in the CS simulation so as to perform the sensitivity analysis. The nested STG1 domain is designed for the finer study of pollution export processes and corresponds to the black square in Fig. 2b (which is a slightly different area than the black rectangle in Fig. 2a). Chemistry is not activated in this domain since the studied compounds are reduced to passive aerosol tracers (fine mode, density of 1.7 g cm^{-3}), distributed over the Santiago Metropolitan Area according to Figure 2b. Tracers emission rates are the same for every location, and can be found in Figure 2c. Emission rates are adapted from HTAP data so as to emit the same total mass of BC as a typical 1 km^2 grid point of the urban area. A daily cycle is then applied on these emission rates to be as close to actual emissions dynamics as possible. Such a configuration allows for the study of the pathways of pollution depending on their origin in the basin, and assess the preferred origin of polluted air masses reaching elevated, snow-covered sites. The nesting between STG1 and CC5 is only used for meteorological conditions simulation purposes in WRF but deactivated for CHIMERE, as the targets in terms of atmospheric composition study differ between the two domains.

3. Contribution of emissions from Santiago to BC deposition

The following analysis estimates the contribution of emissions from Santiago to BC deposition on the nearby Andean snow or ice-covered areas in wintertime. The influence and reach of pollutants emitted in different districts within Santiago is also studied.

3.1. Contribution of the Metropolitan Area

The following analysis is based on the 5 km CC5 CHIMERE simulations. Details of their configuration and validation can be found in Section 2 and Appendix A. Two simulations are compared, one with a full emissions inventory (BS), one where emissions from Santiago area are set to zero (CS). The difference yields an estimate of the share of Santiago's emissions in the atmospheric composition of the region. Snow measurements from Rowe et al. (2019) estimate the surface deposition rate of BC at the *Yerba Loca* site near Santiago (33.33°S, 70.33°W - see YBL in Figure 2b) in July 2016 to around 5.2 mg m^{-2} for the month. For the same location, the baseline simulation (BS) yields 8.7 mg m^{-2} for July 2015, which is comparable in terms of magnitude although these numbers are

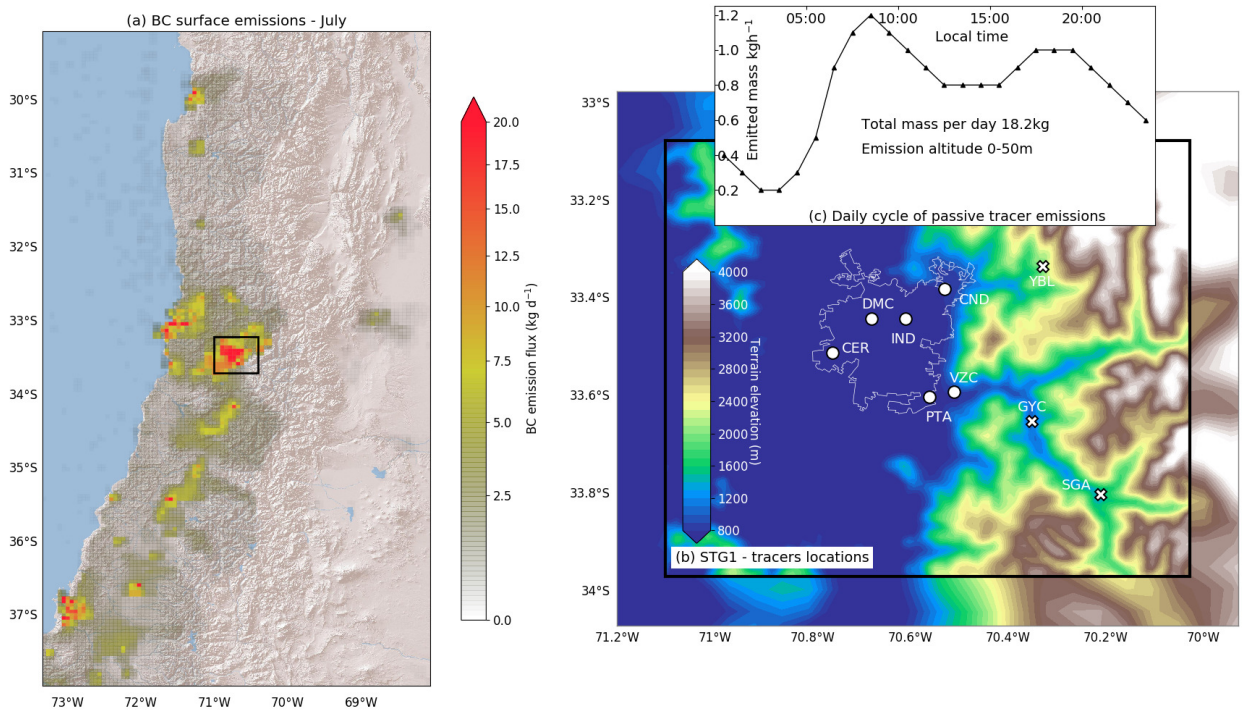

Figure 2: (a) Surface emissions of BC for the CC5 simulation. The black box represents the area where emissions are set to zero for the contribution case. Map background layer: World Shaded Relief, ©2009 ESRI (b) Location of passive aerosol tracers used in the SGT1 simulation (circles) and topography of the basin (colormap). Crosses indicate other relevant locations mentioned in the study. GYC is for *Guyacan*, YBL for *Yerba Loca*, SGA for *San Gabriel* (c) Daily cycle of emission for each tracer.

not for the same years, and despite the relatively coarse resolution of the simulation. We also acknowledge the absence in the EDGAR HTAP emission inventory, of the significant BC source linked to the nearby mining activity at *Los Bronces* (33.15°S, 70.28°W), which may be a source of discrepancy between measurements and modeling, although there is no evidence these emissions reach the site of *Yerba Loca*. Nevertheless, in addition to the good reproduction of meteorology and atmospheric composition observed in Santiago, and despite several sources of uncertainty, having the proper order of magnitude for deposition at this location gives confidence in the behavior of the simulation.

Figure 3 shows the amount (a and b) and proportion (c and d) of the total BC deposition attributable to Santiago emissions for July 2015. This is achieved by representing the difference between the total deposition in the BS case and in the CS case (BS-CS), and the ratio (BS-CS)/BS. Clearly, BC emissions from Santiago mainly affect low elevation areas nearby, particularly regarding dry deposition, with a contribution to BC deposition of 60% to 100%. A significant amount of BC also reaches much higher summits, where it can contribute to up to 40% of the deposition for the period, especially in the southeast of Santiago. Wet deposition is more scarce at this time of the year, and in our case seems driven by orographic precipitation. According to Figure 3b a plausible pattern could be that pollutants from Santiago are blown towards the southeast cordillera consistently with the afternoon westerlies induced by mountain-valley circulation, and are precipitated when moist air masses encounter the foothills and cloud droplets scavenge the air below.

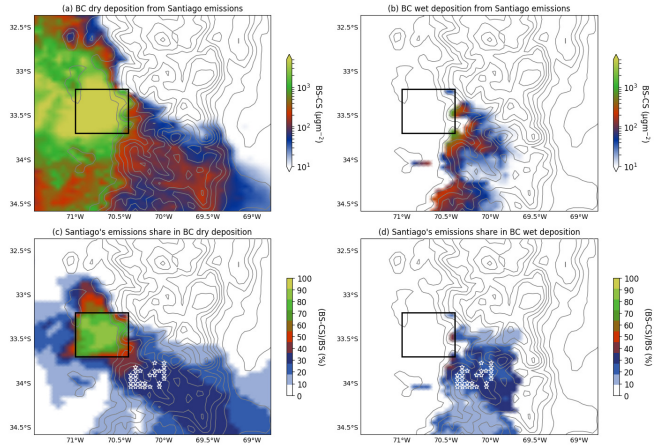

Figure 3: (a) BC dry deposition originating from Santiago's emissions, (b) same as (a) for wet deposition, (c) proportion of BC dry deposition originating from Santiago's emissions, (d) same as (c) for wet deposition. Total over July 2015 - CC5 simulation. The black box corresponds to the area where emissions are set to zero in the CS case. Grey contour levels are every 500 m starting from 1000 m a.s.l. White stars in (c) and (d) show the snow or ice-covered grid points considered in the continuation.

Based on Figure 3, the Andean area most affected by Santiago's emissions during the month of July 2015 is located at the southeast of the city. Accordingly, a focus is made on the terrain in this zone that is permanently snow or ice-covered during the whole month of simulation (grid points shown in white stars in Figures 3c and 3d), to study the temporal evolution of

deposition. From now on, this area is referred to as the target area. The simulated time series of BC dry and wet deposition averaged over the target area is shown in Figures 4a (2-hour deposition) and 4b (accumulated deposition). Dry deposition occurs continuously over the target area during the simulated month, with a marked diurnal cycle but maintaining non-zero values throughout the whole 24-hour cycle, the minimum 2-hour value being $0.2\,\mu g\,m^{-2}$. When the rate of dry deposition is near its minimum, the contribution of emissions from Santiago is very small (solid and dashed line cannot be distinguished), pointing to a domination of local and less intensive sources of BC such as road traffic, mining or wood burning for residential heating in the valley villages. On the other hand, when deposition rates are higher (19 July and 27 July for instance) the contribution of emissions from Santiago becomes more significant reaching up to 50%. BC emissions from Santiago thus seem to play a role mainly during stronger deposition episodes. On the whole, the emissions from the city lead to an accumulated additional dry deposition of $126\,\mu g\,m^{-2}$ (33%) over the target area (Figure 4b). Contrarily to dry deposition which occurs on a continuous basis, only a few precipitation episodes, concentrated between 12 July and 15 July, account for all wet deposition during the month of July 2015. Given the spatial pattern of wet deposition seen in Figure 3b and also the increase in dry deposition right before the precipitation events, this episode likely corresponds to convective moist air masses coming from the northwest, importing BC, and leading to orographic precipitation which in turn scavenges pollutants to the ground. Although slightly weaker than dry deposition, wet deposition of BC from Santiago still accounts for $75\,\mu g\,m^{-2}$ (26%) of total deposition (Figure 4b) and is much more concentrated in time (Figure 4a). As a result, precipitation in wintertime, which have a positive influence on air quality in Santiago because of the associated scavenging of particles, lead at the same time to a higher deposition of light-absorbing particles on snow via wet deposition. Local effects - air quality in Santiago - and global consequences - radiative forcing leading to accelerated melting of glaciers and snow - compete in this regard.

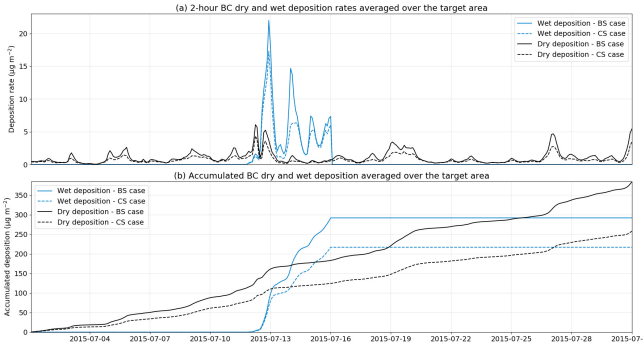

Figure 4: (a) Simulated time series of BC deposition over the target area in the BS case (solid line) and CS case (dashed line), (b) same as (a) but accumulated.

In Figure 4a, the period between 21 to 25 July shows a clear minimum in deposition rate compared to the rest of the time series. In connection, the onset of a coastal low along the subtropical west coast of South America is observed around that period. Figure 5 shows the evolution of the mean sea-level pressure and 925 hPa wind fields between 22 July to 25 July. The patterns correspond well to d-2, d-1, d0 and d+1 of a coastal low event as described in Garreaud et al. (2002). One of the effects of this shallow, warm-core low pressure cell disrupting the synoptic circulation is a strengthening of the easterlies flowing above the Andes (not visible in this large-scale figure) and a strengthening of the persistent inversion layer above Santiago for a few days (Rutllant and Garreaud, 1995; Garreaud et al., 2002). These coastal lows can also affect surface winds through the formation of strong easterly katabatic winds locally known as *raco* (Muñoz et al., 2020, e.g.). As an example, *raco* events were observed on 21 and 24 July (not shown here), during the coastal low development and extinction, and resulted in no deposition coming from Santiago on the Andes, as can be seen in Figure 4a. As a consequence of both phenomena - strong easterlies above the Andes and *raco* - air masses from Santiago are blown in the opposite direction of the Andes when above the mixing layer, and hence do not affect the target area during that period. In parallel, stagnation is favored in the basin, above the urban area. Most wintertime pollution events in the city occur under such synoptic-scale conditions (Rutllant and Garreaud, 1995). Again, conditions favoring urban pollution in Santiago imply minimal export of BC towards the cryosphere.

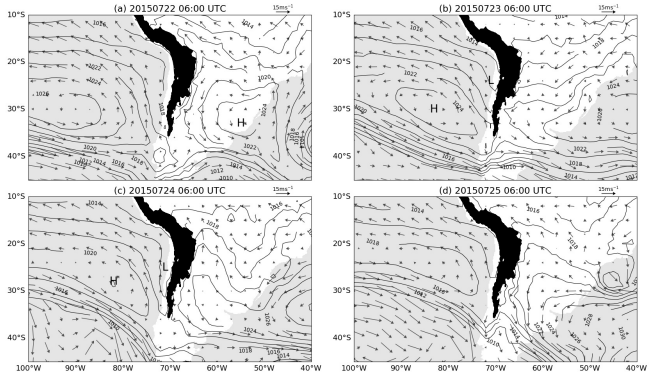

Figure 5: Mean sea-level pressure (contours every 2 hPa) and 925 hPa winds (arrows) at 06:00 UTC from 22 July to 25 July. Data is from the NCEP FNL analysis used as boundary conditions for the CHIMERE simulations. Black area indicates terrain elevation exceeding 2500 m. H and L indicate high and low centers, respectively.

It is clear in these simulations that urban emissions from the capital city of Chile have a significant influence on deposition of light-absorbing particles on Central Andean snow and ice, with an average total deposition of around $200\,\mu g\,m^{-2}$ (corresponding to 30% of the total) on the snow or ice-covered areas southeast of Santiago for the month of July 2015 (Fig. 4). The effect on ice and snow albedo, and thus the associated radiative forcing are not straightforward to estimate. However, the field measurement campaign conducted in the snowpack of the Central Andes by Rowe et al. (2019) found that the regional average vertically-integrated load of BC in snow samples near Santiago was $780\,\mu g\,m^{-2}$, corresponding to a mean radiative forcing of $1.4\,W\,m^{-2}$ during winter. We find that around 30% of this BC is

likely to have been emitted in Santiago (Fig. 4). Hence, a significant fraction of the excess radiative forcing measured in snow samples is attributable to emissions from Santiago, although it is not quantifiable here.

In the above analyses, the metropolitan area of Santiago was considered as a unit block of BC emissions, but this urban area is wide (640 km^2), with large gradients in the spatial distribution of emissions. In addition, the surrounding topography of the Andes makes air masses circulation complex. In this respect, the locations within the Santiago area that have the most impact when it comes to deposition on the Andes, i.e. where pollutants are more likely to reach the glaciers once emitted, are not straightforward. The continuation looks at the locations within Santiago where emissions reductions would imply a significant decrease in BC deposition on the cryosphere.

3.2. Contribution of different districts of Santiago

Using the 1 km resolution STG1 simulation with passive fine mode aerosol tracers, and integrating over the target area (snow or ice-covered - red stars in Figure 6a), the contribution of air masses from different districts of the Santiago Metropolitan Area to atmospheric composition and pollutants deposition on the Andean cryosphere can be studied.

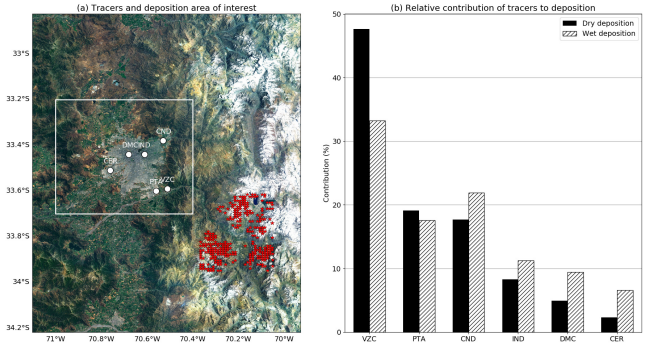

Figure 6: (a) Locations of considered passive tracers (white dots), and target area (red stars) influenced by emissions from Santiago (white box). Map background layer: Imagery World 2D, ©2009 ESRI (b) relative share of each tracer to dry and wet total deposition on the target area for July 2015.

Dry deposition mainly originates from emissions at VZC location (47% of accumulated dry deposition over the month of July), at the entrance of the Maipo canyon (Fig. 6b). Less intuitively, emissions from the northeast (CND - 17%) weigh almost as much as the ones from a site much closer to the target area (PTA - 19%). The other parts of the city considered here, especially downtown, have a lesser role in dry deposition (2% to 8%). Regarding wet deposition, locations of origin are slightly more evenly distributed, indicating a probable role of large-scale convection over the city mixing pollutants and generating clouds. However, only a few precipitation events are simulated over the period, so that concluding on it is not relevant. Generally speaking, Figure 6 shows that the closer the location is to the Andes, regardless of the latitude, the more likely its emitted particles will deposit on the target area. More than proximity to the target area, the interaction of air masses and the foothills and valleys of the cordillera is then of major relevance.

Figure 7 shows the pathways of tracers VZC and CND during the periods 17-20 July and 21-24 July. The former episode features significant deposition on the Andes while the latter shows very little (Fig. 4a). For VZC, an efficient pathway is through the Maipo canyon, southeast of Santiago, that acts as a funnel guiding particles towards the summits during the 17-20 July period (Fig. 7a). The 21-24 July period (Fig. 7c) shows a less marked intrusion in this valley, and the tracer barely reaches high elevation. For CND (Fig. 7b and d) the Mapocho canyon, northeast of Santiago plays a similar role, enabling polluted air masses to enter the network of valleys and eventually access high elevation sites during the 17-20 July period, which occurs much less during the 21-24 July period.

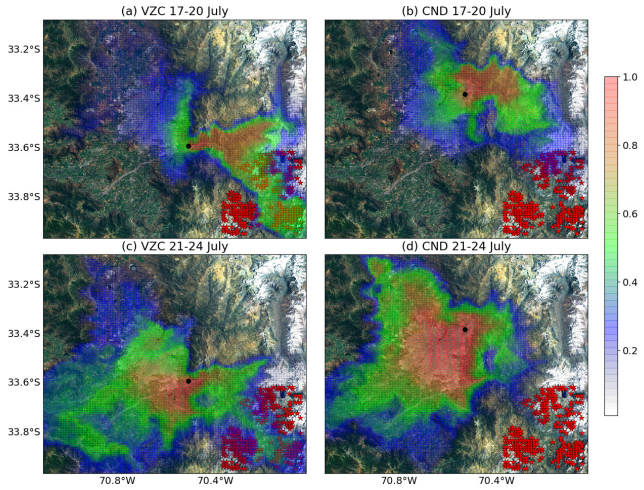

Figure 7: Frequency of tracer surface concentration above 0.2‰ of the maximum concentration at the source for two periods with distinct synoptic circulation (a) VZC for 17-20 July, (c) VZC for 21-24 July, (b) CND for 17-20 July, (d) CND for 21-24 July. Red stars show the target area, black dots the emission site. Map background layer: Imagery World 2D, ©2009 ESRI.

It is important to keep in mind that the results in Figure 6b are based on equal emission rates at every tracer locations. However, actual measurements from the air quality network of Santiago show that the CND location emits much less particulate matter than PTA for instance. The circulation dynamics imply that for each emitted particle at both locations, they have approximately the same likelihood to end up deposited on the cryosphere, but in actual conditions, regulating emissions at PTA would have a much more dramatic impact on deposition given the higher emission rate. Similarly, VZC is found to be at the optimal location, but is also less densely populated and emits less, in total amount, than PTA.

Given the usually stable and subsident conditions in wintertime, and the elevated height of the mountains that are within reach of air masses coming from Santiago (the urban area is only 500 m a.s.l while summits in the southeast, where deposition is observed, can reach up to 4000 m), the processes leading to such a high elevation deposition are not straightforward. Given the previous analysis, a first natural explanation would involve mountain-valley circulation and the so-called mountain venting phenomenon. The latter corresponds to the horizontal advection of air masses from elevated areas towards flat terrain

that, when encountering a shallow mixing layer, leads to the export of boundary layer air into the free troposphere (Kossmann et al., 1999; Henne et al., 2004).

4. Role of the mountain-valley circulation

4.1. Injection of BC into the free troposphere

Circulation and interaction between Santiago and the Maipo canyon, south of Santiago, is studied here. Mountain-valley circulation patterns are clear at this location, with a first part of the canyon being almost zonally oriented (Fig. 6 eastward of VZC), and the second part almost along a meridional axis. Schematically, under usual wintertime conditions, the differential heating of air masses by sunlight between the Santiago basin and the Andean slopes generates an ascending motion of air from the city into the valley during the afternoon, and a reversal of this motion, from the valley towards the city, during nighttime (Fig. 8 and Whiteman (2000)). Since the boundary layer above the city is even shallower at night than during the day, a direct consequence of this circulation pattern is that polluted air masses coming back towards the urban area, if given enough momentum, will likely be injected into the free troposphere (Fig. 8). As a result, pollutants found in this secondary layer above the boundary layer can be exported much farther, and become available on the next day to be transported higher up when the daytime circulation resumes.

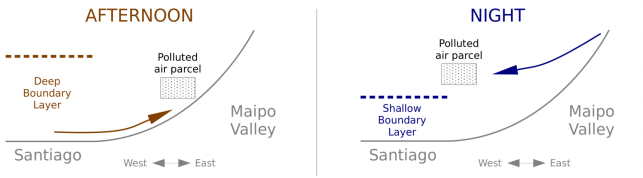

Figure 8: Schematic of the usual mountain-valley circulation along the zonal part of the Maipo canyon and associated venting mechanism.

Such a mechanism was clearly recorded during the 2015 campaign described in Section 2.1, on 22 July at the entrance (VZC) and farther (GYC) in the Maipo canyon (Fig. 2). The combination of a positive zonal wind at VZC and a negative meridional wind at GYC allows for the intrusion of polluted air masses deep into the valley during the afternoon (Fig. 9a). At night, these air masses come back down into the basin (positive meridional wind at GYC and neutral zonal wind at VZC). At 18:00 local time (LT), pollutants at VZC are still contained and well mixed within the boundary layer, while at 21:00 a secondary layer of BC can be observed above the boundary layer (Fig. 9b). The fate of this secondary layer was not observed though, so that validating the hypothesis of injection of the BC higher up as the origin of its transport towards the mountains is not possible with observation only. Our STG1 simulation bridges this gap. It is worth noting that the model (solid lines) agrees reasonably with the observations (dashed lines), both for surface winds at the two locations, and for the shape of the aerosol profile at night, especially regarding the formation of a secondary layer in the free troposphere (Fig. 9). The model generates a shallower mixing layer than observed, but the pattern is consistent.

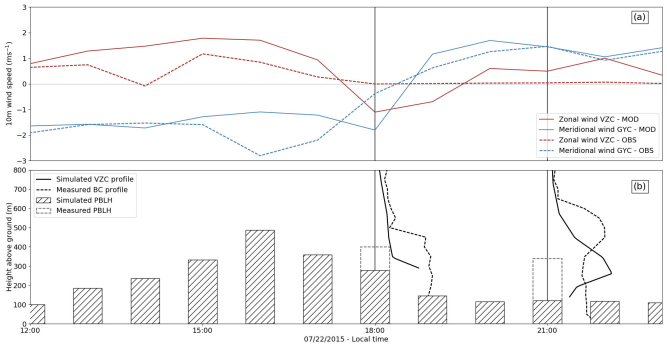

Figure 9: Observed (dashed lines) and modeled (solid lines - STG1 simulation) intrusion episode of 22 July. (a) Observed and modeled zonal wind at VZC and meridional wind at GYC. (b) Boundary layer height and vertical profiles of BC (observed) and VZC tracer (simulated). For the sake of comparability, only the free troposphere profiles are shown for the model. Boundary layer heights from the campaign are derived from vertical profiles based on the methodology described in Stull (1988)

This event can be further described with the STG1 simulation, following along-valley transects of tracers concentrations and wind profiles. At 16:00 LT, particle pollutants, mainly originating from the VZC location, have penetrated deeply into both branches of the Maipo canyon, mostly within the boundary layer (Fig. A.2). This intrusion is mainly driven by low-level winds in both valleys, while a wind shear at the end of the southern valley disconnects the polluted air masses from the surface. 5 hours later (Fig. A.3) low-level winds have reversed, consistently with mountain-valley circulation, and blow tracer-containing air masses back towards the Santiago basin. However, while the intrusion was governed mostly by surface winds, winds above the boundary layer now dominate the advection. As a result, particles are injected into the free troposphere over Santiago, as already evidenced in Figure 9. Thus, despite stable conditions and a shallow boundary layer, the mountain valley circulation allows for the export of pollutants higher up.

However, when tracking the secondary layer of BC injected into the free troposphere, it does not appear to go back into the direction of the Andes, but rather continue its path towards the west of Santiago, and eventually be diluted without being recovered higher up despite winds above 2000 m blowing in the favorable direction (Fig. A.4). This result is consistent with the time series in Figure 4a, where almost no deposition occurs on the target area in the few hours following the 22 July venting episode. In fact, the whole period between 22 July and 25 July in Figure 4a features very little deposition. This can be traced back to the onset of the coastal low, as discussed in Section 3.1. The hypothesis of the observed secondary layer of pollution in the free troposphere as a source of export and deposition of BC, does not apply in this case. Nevertheless, while the nighttime venting may not be relevant, the daytime mechanism of injection of pollutants into the Andean valleys is critical.

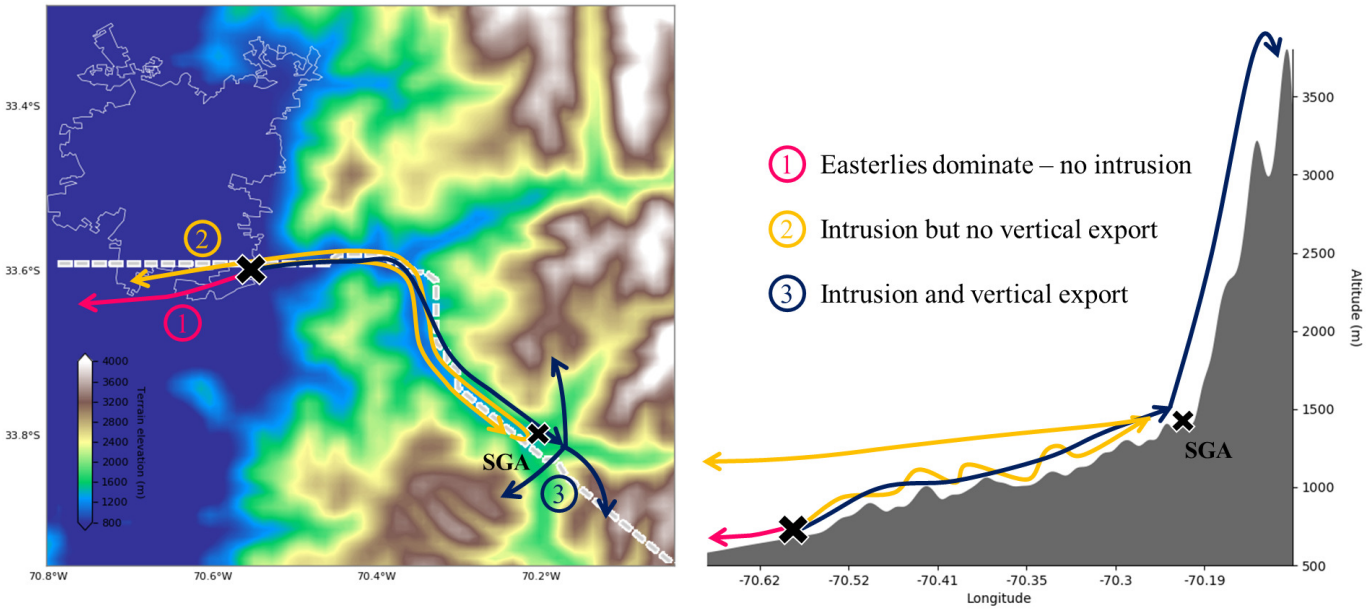

Figure 10: Schematic of the 3 export situations from a latitude/longitude (left) altitude/longitude (right) perspective. The transect followed in the right-hand panel is shown in white dashed line in the left-hand panel.

4.2. *Valley intrusion of air masses and vertical export*

When comparing the two contrasted periods mentioned in Section 3.2, although the total deposition over the whole domain remains similar (7% difference on the accumulated deposition of tracers), the spatial patterns greatly differ. As seen in Figure 7, during the 21-24 July period, pollutants are advected towards the city and the southwest region mainly, while during the 17-20 July period they are found in the northwest, the east of Santiago adjacent to the cordillera, and over the Andes. Section 4.1 points towards two key meteorological components of the mountain-valley circulation driving the fate of polluted air masses: the low-level zonal wind above the city, and the vertical motions at the end of the southern valley. Schematically, the weak vertical mixing associated with wintertime conditions forces the pollutants to follow a pathway along gentle slopes near the ground to reach or get closer to the snow or ice-covered areas. Furthermore, even though events of polluted air intrusion into the Maipo canyon occur, these air masses do not necessarily reach the snow or ice-covered areas of the Andes. Based on the above, we identify three possible transport alternatives which are schematically represented in Figure 10: (1) easterly winds dominate and urban polluted air masses are transported away from the Andes, (2) westerlies enable intrusion into the canyon but pollutants cannot reach the Andean cryosphere and (3) deep intrusion occurs and air masses are successfully transported to the Andean summits. The latter is the case where we expect large deposition.

We derive now a parameterization indicating the likelihood that one of the aforementioned alternatives occur and we use the simulated daily deposition of tracers in July 2015 to examine its validity. Given the fact that the chance of an air mass reaching the Andean cryosphere is linked first to the occurrence of a zonal wind transporting the air parcels into the canyon and then lifting it to the Andean summits, we choose the simulated near-surface zonal wind (u) over the Santiago basin in the afternoon to represent the former and the simulated vertical diffusion coefficient (K_z) near the surface in the valley, close to the summits, at the same time of day to express the magnitude of vertical motion. The combination of these parameters evidences that large deposition occurs for significant zonal winds and vertical diffusion (large circles in Fig. 11a). For strong zonal winds only or strong updrafts only, deposition is moderate. For situations with both weak winds and vertical diffusion, almost no deposition occurs.

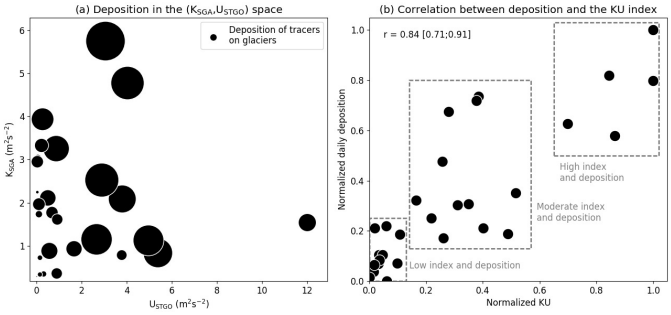

Figure 11: (a) Tracers dry deposition on the target area dependency on K_{SGA} and U_{STGO}. Circles areas are proportional to deposition. (b) Relationship between the normalized daily dry deposition and the normalized index $KU/\max(KU)$. The correlation is given with a 95% confidence interval.

The parameterization combining these two variables, representing the above and thus expressing the likelihood of occurrence of deposition is defined in Eq. 1. For the K_z term we choose the vertical diffusion coefficient at 40 m above ground level at the location of San Gabriel (K_{SGA} - see SGA in Figures 2 and 10) averaged between 14:00 and 20:00 LT. San Gabriel is

considered because of its location at the end of the main southern valley where the pollutants are lifted from the ground to the Andean summits (Fig. A.2b). For the zonal wind component (u) we choose the zonal wind at 40 m above ground level, squared and averaged over the urban area of Santiago and between 14:00 and 20:00 LT (hereafter U_{STGO}). The zonal wind is squared so as to be homogeneous to a kinetic energy per unit mass of air, which is what physically provides momentum for the intrusion of air masses. Both U_{STGO} and K_{SGA} are capped, related to the fact that above a certain threshold, increasing wind speed or vertical motion does not bring any more deposition if the other parameter is too small, as evidenced in Figure 11a. The thresholds are empirically set to $1\,\mathrm{m\,s^{-1}}$ for u and $3\,\mathrm{m^2\,s^{-2}}$ for K_z. The correlation of this index with dry deposition is illustrated in Figure 11b. The deposition term considered here is limited to the target area summed for all tracers between 14:00 and 04:00 LT, and normalized by the maximum deposition over the period. The resulting correlation is not very sensitive to the choice of the threshold values for U_{STGO} and K_{SGA} as long as they are not taken too small, and such thresholds are necessary to have a consistent result. This index accounts for (i) intrusion of urban BC into the Maipo canyon via significant zonal winds over the city in the afternoon (ii) the possibility for air masses to be exported from the bottom of the valley up to the summits at the same time, before being distributed and diluted into several smaller valleys. Combining (i) and (ii) leads to large deposition a few hours later (hence the consideration for the total deposition between 14:00 and 04:00 LT). Having only one of the two induces moderate deposition, having none leads to limited to no deposition. This justifies the choice of multiplying the two variables, accounting for a logical *and* relationship, although the meteorological meaning of the resulting index is not obvious. The correlation between the normalized deposition and normalized KU is 0.84 [0.71;0.91] at the 95% confidence level, showing that the combination of positive zonal winds in the basin and vertical diffusion in the deep valley accounts for most dry deposition episodes (top right corner box in Figure 11b). It is worth noting that the contribution of each tracer source in high deposition days follows the average distribution found in Figure 6b, with dominance from VZC, and CND and PTA playing similar roles at round 20%. Conversely, when both wind and K_z are low, almost no deposition occurs (bottom left corner box in Figure 11b). For intermediate values of the two variables, deposition is more scattered but remains within median values. A corollary of this strong correlation is that the detachment of pollutants from the surface is driven by mixing and turbulence processes deep in the valleys network, rather than by organized circulation patterns.

$$\begin{aligned} KU &= K_{SGA} \times U_{STGO} \\ &= \min(< Kz_{SGA} >_{14-20}; 3) \times \min(< u^2{}_{STGO} >_{14-20}; 1) \end{aligned} \quad (1)$$

5. Discussion

Although this study looks into one particular month, there are reasons to believe that the results are more general. Indeed, Figure A.1 shows that July 2015 is climatologically relevant given the usual character of its meteorological conditions for winter months. Besides, although a quantitative analysis is performed specifically for July 2015, the qualitative results determining the critical meteorological variables and the pathways associated with export and deposition of pollutants on the cordillera can be generalized to all winter months. In addition, the year-to-year variability in BC emissions is not significant for Santiago at the monthly level, except for particular peak events such as the ones described in Lapere et al. (2020). However those peak events occur at night so that air masses cannot be exported into the Andean canyons. Traffic and residential heating provide most of the BC. The former does not change much from year-to-year and the latter is mainly connected to outside temperatures, for which July 2015 is not an outlier. Thus, the magnitude of exported and deposited BC on the cryosphere every year is likely around the estimate given in Section 3.1 for dry deposition. Wet deposition might be more variable from one year to another. The pathways identified here for a particular valley likely apply for other valleys in the area, although this calls for further research.

The present work focuses on wintertime conditions because they combine high BC emissions due to residential heating with wood burning, and a large extent of snow covered areas. However, it is worth briefly discussing what could be expected for other seasons in terms of export pathways and deposition. May/June/July/August concentrate most of the annual precipitation in Central Chile with an average $59\,\mathrm{mm\,month^{-1}}$ while November/December/January/February only see precipitation of $3.5\,\mathrm{mm\,month^{-1}}$ on average in downtown Santiago (data for the period 1950-2019 from the CR2 database for station *Quinta Normal* - see Section 2.1 for the data source). As a result, wet deposition is not expected to be a recurring process of export and removal of BC from the atmosphere in spring and summer seasons. Regarding atmospheric export and dry deposition, the warmer periods of the year feature a more turbulent atmosphere, with a much deeper mixing layer. A consequence is the greater ability for BC particles to be exported higher up and reach more elevated areas so far as to travel over the Andes towards Argentina more easily. On the other hand, more turbulence means that a larger fraction of BC is also brought back to the ground by downdrafts, and that the mountain-valley circulation might be overcome by these turbulent motions making deposition on the Andes less periodic. Again this is just a glimpse at what we expect since other seasons are not within the scope of this work, but these are the features that should be investigated.

To obtain the deposition rate estimate, a 5 km resolution chemistry-transport simulation is performed. Such a resolution is relatively coarse given the sharp orography of the studied area. Valleys are not necessarily well reproduced, and mountain ranges are flattened, appearing lower than they are because of sub-grid averaging. Nevertheless, Section 2.2 showed that the

performance of the model is still good, and in particular it has the ability to capture well the deposition rate of BC on snow measured at an Andean site. Still, the quantitative results from simulation CC5 are not to be taken as definitive, but we have good confidence that the order of magnitude is realistic. This is only a first step and more work needs to be done, but the results obtained so far show that the model reproduces deposition fluxes and that the approach is promising to extend them and to examine other valleys and periods of the year.

Throughout the study, the idea emerged that the conditions preventing BC deposition on the Andes are the ones that lead to high urban pollution in the city and vice versa (coastal lows strengthening inversions versus enhanced zonal winds). Although a qualitative explanation was given, it is also possible to quantify this relationship with the CHIMERE simulation data. In the model outputs, the correlation between the daily average BC concentration at IND location (downtown Santiago - see Figure 2), and the daily average deposition of BC on the target area is -0.58 [-0.63;-0.51] at the 95% level. This number illustrates the idea that urban pollution and deposition on the cryosphere are anti-correlated despite their sharing the same sources. This phenomenon is explained by the fact that if the meteorological conditions do not allow for the export of pollutants (i.e. no wind and/or presence of a coastal low) then particulate matter accumulates over Santiago without the possibility of export. A result of such conditions is (i) high concentrations of pollutants in Santiago due to accumulation (ii) no deposition on the glaciers for the period that follows because pollutants are not able to export and remain above the urban area and hence cannot reach the Andes. More favorable export conditions result in the exact opposite with a renewal of air masses in Santiago when polluted ones are exported, thus explaining the observed anti-correlation.

6. Conclusions

In wintertime, light-absorbing particles such as BC are massively emitted in the metropolitan area of Santiago. Measurements in the literature show significant amounts of BC in snow in the Andes near Santiago, but the contribution of the city was never estimated. Based on chemistry-transport simulations, we show that urban emissions can contribute to up to 40% of BC deposition on southeastern snow or ice-covered areas of the Central Andes, corresponding to $200\,\mu g\,m^{-2}$ for the month of July 2015, with a potential dramatic radiative impact. Despite rather stable conditions in wintertime, we show that an essential role is played by up-slope winds, i.e. mostly zonal winds, in the afternoon, that carry polluted air masses deep inside the Maipo and Mapocho canyons. If the vertical motions in the valley allow for the export of these polluted masses, they can then access higher elevations and deposit on the snowpack and glaciers. Quantitatively speaking, as soon as zonal winds over Santiago exceed $1\,m\,s^{-1}$ on average in the afternoon, and the vertical diffusion coefficient at the tip of the Maipo valley is higher than $3\,m^2\,s^{-2}$, large amounts of BC are expected to deposit on snow or ice-covered areas. Contrarily, large scale strengthening of easterlies over the Andes, as generated during coastal lows and associated with enhanced subsidence, are linked with decreased export and deposition of pollution towards the mountains. All districts of the Metropolitan Area do not have the same influence on air masses reaching the Andes. As a result, great attention must be paid to emission control policies in this respect. Finally, we show that urban pollution and deposition on the cryosphere are anti-correlated: large BC concentrations at downtown Santiago coincide in general with weak deposition fluxes on the target area and vice versa. These results provide additional information to enrich mitigation policies allowing them not only design measures improving air quality in Santiago but also to mitigate the urban impact on the nearby cryosphere. Although the present study focuses on the area of Santiago, such a configuration involving large urban basins close to the Andean slopes can be found at numerous latitudes along the cordillera. As a result, our conclusions provide a basis to guide further investigation, over a broader area, particularly in the context of the critical need for a thoroughly-informed management of water resources in all Andean countries.

Declaration of competing interests

The authors declare that they have no known competing financial interests or personal relationships that could have appeared to influence the work reported in this paper.

Acknowledgments

The chemistry-transport simulations used in this work were performed using the high-performance computing resources of TGCC (Très Grand Centre de Calcul du CEA) under the allocation GEN10274 provided by GENCI (Grand Équipement National de Calcul Intensif). NH was partially funded by FONDECYT Regular project 1181139 and Research and Innovation programs under grant agreement no 870301 (AQ-WATCH). NH acknowledges the support of project ANID-PIA-Anillo INACH ACT192057 and MAP-AQ which is an IGAC and WMO sponsored activity. The research leading to these results has received funding from the European Union H2020 program PAPILA (GA 777544). Measurements at VZC were possible with the collaboration of Colegio Almenar del Maipo. The authors acknowledge the precious comments and suggestions of the two anonymous reviewers and the editor.

Authors contributions

NH provided the 2015 campaign data and analysis. As developers of CHIMERE, LM and SM supervised the chemistry transport simulations and analyses of the results. RL performed the conceptualization, data analysis and model simulations, and coordinated the writing of the paper with LM, SM and NH.

Code availability

The CHIMERE model used can be found at `http://www.lmd.polytechnique.fr/chimere/CW-download.php` (last

access 28 April 2020). The WRF model used can be found at http://www2.mmm.ucar.edu/wrf/users/download/get_source.html (last access 28 April 2020).

Data availability

Surface observation data used in this study are available at https://sinca.mma.gob.cl/index.php/region/index/id/M (last access 28 April 2020). HTAP raw emission inventory can be downloaded at http://edgar.jrc.ec.europa.eu/htap_v2/ (last access 28 April 2020). Other data can be made available from the corresponding author upon reasonable request.

References

F. Barraza, F. Lambert, H. Jorquera, A. M. Villalobos, and L. Gallardo. Temporal evolution of main ambient $PM_{2.5}$ sources in Santiago, Chile, from 1998 to 2012. *Atmos. Chem. Phys.*, 17:10093–10107, 2017. doi: 10.5194/acp-17-10093-2017.

F. Cereceda-Balic, M. R. Palomo-Marín, E. Bernalte, V. Vidal, J. Christie, X. Fadic, J. L. Guevara, C. Miro, and E. Pinilla Gil. Impact of Santiago de Chile urban atmospheric pollution on anthropogenic trace elements enrichment in snow precipitation at Cerro Colorado, Central Andes. *Atmos. Environ.*, 47:51–57, 2011. doi: 10.1016/j.atmosenv.2011.11.045.

A. M. Cordova, J. Arévalo, J. C. Marín, D. Baumgardner, G. B. Raga, D. Pozo, C. A. Ochoa, and R. Rondanelli. On the Transport of Urban Pollution in an Andean Mountain Valley. *Aerosol Air Qual. Res.*, 16:593–605, 2015. doi: 10.4209/aaqr.2015.05.0371.

H. Diémoz, F. Barnaba, T. Magri, G. Pession, D. Dionisi, S. Pittavino, I. K. F. Tombolato, M. Campanelli, L. S. Della Ceca, M. Hervo, L. Di Liberto, L. Ferrero, and G. P. Gobbi. Transport of Po Valley aerosol pollution to the northwestern Alps - Part 1: Phenomenology. *Atmos. Chem. Phys.*, 19: 3065–3095, 2019a. doi: 10.5194/acp-19-3065-2019.

H. Diémoz, G. P. Gobbi, T. Magri, G. Pession, S. Pittavino, I. K. F. Tombolato, M. Campanelli, and F. Barnaba. Transport of Po Valley aerosol pollution to the northwestern Alps - Part 2: Long-term impact on air quality. *Atmos. Chem. Phys. Discuss*, submitted, 2019b. doi: 10.5194/acp-19-10129-2019.

M. A. Friedl, D. Sulla-Menashe, B. Tan, A. Schneider, N. Ramankutty, A. Sibley, and X. Huang. MODIS Collection 5 global land cover: Algorithm refinements and characterization of new datasets, 2001-2012, Collection 5.1 IGBP Land Cover, 2010. URL http://lpdaac.usgs.gov.

R. D. Garreaud. The Andes climate and weather. *Adv. Geosci.*, 22:3–11, 2009. doi: 10.5194/adgeo-22-3-2009.

R. D. Garreaud, J. A. Ruttlant, and H. Fuenzalida. Coastal Lows along the Subtropical West Coast of South America: Mean Structure and Evolution. *Mon. Weather Rev.*, 130:75–88, 2002. doi: 10.1175/1520-0493(2002)130⟨0075:CLATSW⟩2.0.CO;2.

R. D. Garreaud, C. Alvarez-Garreton, J. Barichivich, J. P. Boisier, D. Christie, M. Galleguillos, C. LeQuesne, J. McPhee, and M. Zambrano-Bigiarini. The 2010-2015 megadrought in central Chile: impacts on regional hydroclimate and vegetation. *Hydrol. Earth Syst. Sci.*, 21:6307–6327, 2017. doi: 10.5194/hess-21-6307-2017.

R. D. Garreaud, J. P. Boisier, R. Rondanelli, A. Montecinos, H. H. Sepúlveda, and D. Veloso-Aguila. The Central Chile Mega Drought (2010-2018): A climate dynamics perspective. *Int. J. Climatol.*, 40:421–439, 2019. doi: 10.1002/joc.6219.

E. Gramsch, A. Muñoz, J. Langner, L. Morales, C. Soto, P. Pérez, and M. A. Rubio. Black carbon transport between Santiago de Chile and glaciers in the Andes Mountains. *Atmos. Environ.*, 232:117546, 2020. doi: 10.1016/j.atmosenv.2020.117546.

S. Henne, M. Furger, S. Nyeki, M. Steinbacher, B. Neininger, S. F. J. de Wekker, J. Dommen, N. Spichtinger, A. Stohl, and A. S. H. Prévôt. Quantification of topographic venting of boundary layer air to the free troposphere. *Atmos. Chem. Phys.*, 4:497–509, 2004. doi: 10.5194/acp-4-497-2004.

R. Hock, G. Rasul, C. Adler, B. Cáceres, S. Gruber, Y. Hirabayashi, M. Jackson, A. Kääb, S. Kang, S. Kutuzov, A. Milner, U. Molau, S. Morin, B. Orlove, and H. Steltzer. *High Mountain Areas*. In: IPCC Special Report on the Ocean and Cryosphere in a Changing Climate [H.-O. Pörtner, D. C. Roberts, V. Masson-Delmotte, P. Zhai, M. Tignor, E. Poloczanska, K. Mintenbeck, A. Alegría, M. Nicolai, A. Okem, J. Petzold, B. Rama, N. M. Weyer (eds.)]. In press., 2019.

H. A. Holmes, J. K. Sriramasamudram, E. R. Pardyjak, and C. D. Whiteman. Turbulent Fluxes and Pollutant Mixing during Wintertime Air Pollution Episodes in Complex Terrain. *Environ. Sci. Technol.*, 49:13206–13214, 2015. doi: 10.1021/acs.est.5b02616.

G. Janssens-Maenhout, M. Crippa, D. Guizzardi, F. Dentener, M. Muntean, G. Pouliot, T. Keating, Q. Zhang, J. Kurokawa, R. Wankmüller, H. Denier van der Gon, J. J. P. Kuenen, Z. Klimont, G. Frost, S. Darras, B. Koffi, and M. Li. HTAPv2.2: a mosaic of regional and global emission grid maps for 2008 and 2010 to study hemispheric transport of air pollution. *Atmos. Chem. Phys.*, 15:11411–11432, 2015. doi: 10.5194/acp-15-11411-2015.

S. Kang, Y. Zhang, Y. Qian, and H. Wang. A review of black carbon in snow and ice and its impact on the cryosphere. *Earth-Sci. Rev.*, page In press, 2020. doi: 10.1016/j.earscirev.2020.103346.

M. Kossmann, U. Corsmeier, S. F. J. De Wekker, F. Fiedler, R. Vögtlin, N. Kalthoff, H. Güsten, and B. Neininger. Observations of handover processes between the atmospheric boundary layer and the free troposphere over mountainous terrain. *Contributions to Atmospheric Physics*, 72:329–350, 1999.

R. Lapere, L. Menut, S. Mailler, and N. Huneeus. Soccer games and record breaking $PM_{2.5}$ pollution events in Santiago, Chile. *Atmos. Chem. Phys.*, 20:4681–4694, 2020. doi: 10.5194/acp-20-4681-2020.

S. Mailler, L. Menut, D. Khvorostyanov, M. Valari, F. Couvidat, G. Siour, S. Turquety, R. Briant, P. Tuccella, B. Bessagnet, A. Colette, L. Létinois, K. Markakis, and F. Meleux. CHIMERE-2017: from urban to hemispheric chemistry-transport modeling. *Geosci. Model Dev.*, 10:2397–2423, 2017. doi: 10.5194/gmd-10-2397-2017.

M. Ménégoz, G. Krinner, Y. Balkanski, A. Cozic, O. Boucher, and P. Ciais. Boreal and temperate snow cover variations induced by black carbon emissions in the middle of the 21st century. *The Cryosphere*, 7:537–554, 2013. doi: 10.5194/tc-7-537-2013.

M. Ménégoz, G. Krinner, Y. Balkanski, O. Boucher, A. Cozic, S. Lim, P. Ginot, P. Laj, H. Gallée, P. Wagnon, A. Marinoni, and H. W. Jacobi. Snow cover sensitivity to black carbon deposition in the Himalayas: from atmospheric and ice core measurements to regional climate simulations. *Atmos. Chem. Phys.*, 14:4237–4249, 2014. doi: 10.5194/acp-14-4237-2014.

L. Menut, B. Bessagnet, D. Khvorostyanov, M. Beekmann, N. Blond, A. Colette, I. Coll, G. Curci, G. Foret, A. Hodzic, S. Mailler, F. Meleux, J.-L. Monge, I. Pison, G. Siour, S. Turquety, M. Valari, R. Vautard, and M. G. Vivanco. CHIMERE 2013: a model for regional atmospheric composition modelling. *Geosci. Model Dev.*, 6:981–1028, 2013. doi: 10.5194/gmd-6-981-2013.

J. Ming, C. Xiao, Z. Du, and X. Yang. An overview of black carbon deposition in High Asia glaciers and its impacts on radiation balance. *Advances in Water Resources*, 55:80–87, 2012. doi: 10.1016/j.advwatres.2012.05.015.

L. T. Molina, L. Gallardo, M. Andrade, D. Baumgardner, M. Borbor-Córdova, R. Bórquez, G. Casassa, F. Cereceda-Balic, L. Dawidowski, R. Garreaud, N. Huneeus, F. Lambert, J. L. McCarty, J. Mc Phee, M. Mena-Carrasco, G. B. Raga, C. Schmitt, and J. P. Schwarz. Pollution and its impacts on the South American Cryosphere (PISAC). *Earth's Future*, 3:345–369, 2015. doi: 10.1002/2015EF000311.

R. C. Muñoz, L. Armi, J. A. Rutllant, M. Falvey, C. D. Whiteman, R. D. Garreaud, A. Arriagada, F. Flores, and N. Donoso. Raco Wind at the Exit of the Maipo Canyon in Central Chile: Climatology, Special Observations, and Possible Mechanisms. *J. Appl. Meteor. Climatol.*, 59:725–749, 2020. doi: 10.1175/JAMC-D-19-0188.1.

NCEP. NCEP FNL Operational Model Global Tropospheric Analyses, continuing from July 1999, 2000. URL https://doi.org/10.5065/D6M043C6.

F. Pellicciotti, S. Ragettli, M. Carenzo, and J. McPhee. Changes of glaciers in the Andes of Chile and priorities for future work. *Sci. Tot. Environ.*, 493: 1197–1210, 2013. doi: 10.1016/j.scitotenv.2013.10.055.

P. M. Rowe, R. R. Cordero, S. G. Warren, E. Stewart, S. J. Doherty, A. Pankow, M. Schrempf, G. Casassa, J. Carrasco, J. Pizarro, S. MacDonell, A. Damiani, F. Lambert, R. Rondanelli, N. Huneeus, F. Fernandoy, and S. Neshyba. Black carbon and other light-absorbing impurities in snow in the Chilean

Andes. *Sci. Rep.*, 9:4008, 2019. doi: 10.1038/s41598-019-39312-0.

J. A. Rutllant and R. D. Garreaud. Meteorological Air Pollution Potential for Santiago, Chile: Towards an Objective Episode Forecasting. *Environ. Monit. Assess.*, 34:223–244, 1995. doi: 10.1007/BF00554796.

W. C. Skamarock, J. B. Klemp, J. Dudhia, D. O. Gill, D. M. Barker, M. G. Duda, X.-Y. Huang, W. Wang, and J. G. Powers. A Description of the Advanced Research WRF Version 3. *NCAR Technical Note*, 27, 2008.

R. B. Stull. *An Introduction to Boundary Layer Meteorology*. Atmospheric and Oceanographic Sciences Library. Springer Netherlands, 1988. ISBN 9789027727695.

D. C. Whiteman. *Mountain Meteorology: Fundamentals and Applications*. Oxford University Press, 2000.

Y. Zhang, S. Kang, Z. Cong, J. Schmale, M. Sprenger, C. Li, W. Yang, T. Gao, M. Sillanpää, X. Li, Y. Liu, P. Chen, and X. Zhang. Light-absorbing impurities enhance glacier albedo reduction in the southeastern Tibetan plateau. *J. Geophys. Res. Atmos.*, 122:6915–6933, 2017. doi: 10.1002/2016JD026397.

Appendix A.

WRF configuration		CHIMERE configuration	
Coarse domain resolution	5 km	Coarse domain resolution	5km
Nested domain resolution	1 km	Nested domain resolution	1km
Vertical levels	46	Vertical levels	30
Microphysics	WSM3	Chemistry	MELCHIOR
Boundary and surface layer	MYNN	Gas/Aerosol Partition	ISORROPIA
Land surface	Noah LSM	Horizontal Advection	Van Leer
Cumulus parameterization	Grell G3	Vertical Advection	Upwind
Longwave radiation	CAM	Boundary Conditions	LMDz-INCA + GOCART
Shortwave radiation	Dudhia		

Table A.1: WRF and CHIMERE configurations

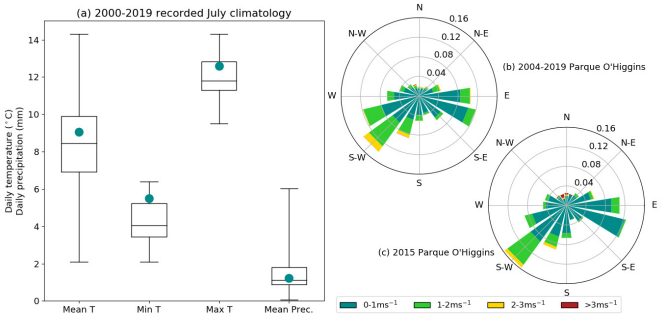

Figure A.1: (a) Daily 2 m air temperature (average, minimum and maximum) and precipitation (average) distribution for 2000-2019 at DMC (33.44°S,70.68°W). Values for 2015 are shown in blue dots. Source CR2. (b) Hourly 10 m wind speed at Parque O'Higgins (33.45°S,70.66°W), 2004-2019. Source SINCA. (c) Same as (b) for 2015 only.

Station:	Las Condes				Independencia		
	MB	NRMSE	R		MB	NRMSE	R
TEMP	NA	NA	NA	:	-0.17 | -0.18	0.08 | 0.08	0.91 | 0.91
RH	-20.64 | -18.07	0.28 | 0.25	0.83 | 0.86	:	-19.84 | -19.60	0.27 | 0.26	0.83 | 0.83
U10m	0.39 | 0.81	0.15 | 0.21	0.54 | 0.25	:	-0.31 | -0.13	0.74 | 0.64	0.41 | 0.41
V10m	-0.01 | -0.12	0.18 | 0.22	0.54 | 0.53	:	0.46 | 0.55	0.14 | 0.15	0.60 | 0.62
Station:	Pudahuel				Puente Alto		
	MB	NRMSE	R		MB	NRMSE	R
TEMP	-0.30 | 0.06	0.09 | 0.09	0.92 | 0.92	:	2.12 | 2.31	0.11 | 0.12	0.93 | 0.93
RH	-21.05 | -22.18	0.31 | 0.32	0.76 | 0.77	:	-19.29 | -19.83	0.27 | 0.28	0.83 | 0.83
U10m	-0.40 | -0.36	0.22 | 0.22	0.27 | 0.19	:	-0.40 | -0.44	0.14 | 0.14	0.73 | 0.71
V10m	0.11 | 0.32	0.11 | 0.12	0.66 | 0.64	:	0.06 | 0.21	0.12 | 0.12	0.39 | 0.41

Table A.2: Simulation scores for hourly surface meteorology. 1 July to 31 July 2015. Left column values are for CC5, right ones for STG1. MB is mean bias, NRMSE is normalized root mean square error and R is Pearson correlation. TEMP is the 2 m air temperature, RH is relative humidity, U10m and V10m are zonal and meridional wind speed at 10 m, respectively.

Day:	21 July 2015				24 July 2015				25 July 2015		
	MB	RMSE	R		MB	RMSE	R		MB	RMSE	R
TEMP	-0.23	0.03	1.0	:	2.44	0.09	1.0	:	1.19	0.07	1.0
RH	-13.12	0.27	0.84	:	-1.65	0.39	-0.13	:	-2.39	0.19	0.87
U	1.76	0.19	0.9	:	-0.57	0.13	0.92	:	0.48	0.17	0.88
V	0.21	0.17	0.84	:	-0.44	0.11	0.95	:	1.91	0.17	0.95

Table A.3: Simulation scores for meteorological vertical profiles at 12:00 LT for 3 days at DMC station in Santiago. STG1 simulation.

Station:	Las Condes				Independencia		
	MB	NRMSE	R		MB	NRMSE	R
Daily $PM_{2.5}$	-8.71	0.32	0.11	:	12.68	0.27	0.69
Hourly $PM_{2.5}$	-8.45	0.17	0.33	:	12.74	0.25	0.57
Station:	Pudahuel				Puente Alto		
	MB	NRMSE	R		MB	NRMSE	R
Daily $PM_{2.5}$	16.69	0.32	0.53	:	-6.62	0.27	0.57
Hourly $PM_{2.5}$	16.77	0.22	0.37	:	-6.45	0.17	0.32

Table A.4: Simulation scores for surface $PM_{2.5}$ concentrations for CC5. 1 July to 31 July 2015.

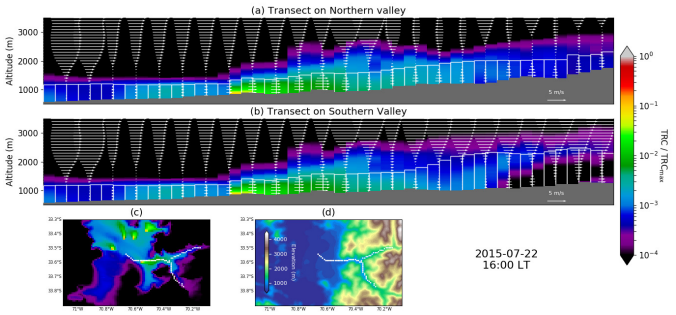

Figure A.2: (a) Transect of normalized tracers concentration (colormap), along-valley horizontal wind profiles (white arrows) and boundary layer height (white bars) along the northern part of the Maipo canyon. (b) Same as (a) for the southern part of the Maipo canyon. (c) Ground level normalized concentrations of all tracers. White dots show the transect paths. (d) Terrain elevation map. Snapshot on 22 July at 16:00 LT.

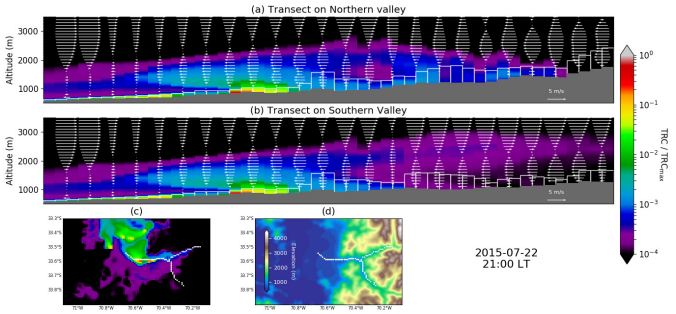

Figure A.3: Same as Figure A.2 but on 22 July at 21:00 LT.

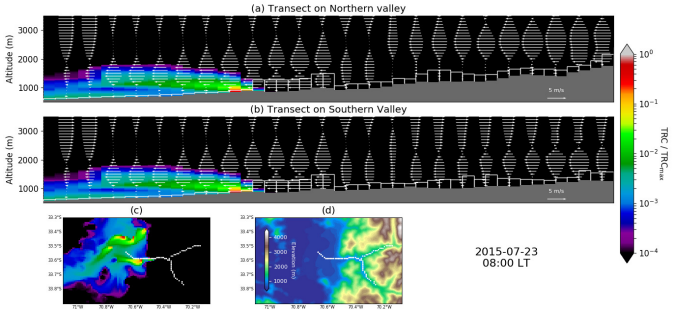

Figure A.4: Same as Figures A.2 and A.3 but on 23 July at 08:00 LT.